

# Enabling Passive Backscatter Tag Localization Without Active Receivers

Abeer Ahmad, Xiao Sha, Milutin Stanačević, Akshay Athalye, Petar M. Djurić, Samir R. Das

Stony Brook University  
Stony Brook, New York 11794, U.S.A.

## ABSTRACT

Backscattering tags transmit passively without an on-board active radio transmitter. Almost all present-day backscatter systems, however, rely on active radio receivers. This presents a significant scalability, power and cost challenge for backscatter systems. To overcome this barrier, recent research has empowered these passive tags with the ability to reliably receive backscatter signals from other tags. This forms the building block of passive networks wherein tags talk to each other without an active radio on either the transmit or receive side. For wider functionality, accurate localization of such tags is critical. All known backscatter tag localization techniques rely on active receivers for measuring and characterizing the received signal. As a result, they cannot be directly applied to passive tag-to-tag networks. This paper overcomes the gap by developing a localization technique for such passive networks based on a novel method for phase-based ranging in passive receivers. This method allows pairs of passive tags to collaboratively determine the inter-tag channel phase while effectively minimizing the effects of multipath and noise in the surrounding environment. Building on this, we develop a localization technique that benefits from large link diversity uniquely available in a passive tag-to-tag network. We evaluate the performance of our techniques with extensive micro-benchmarking experiments in an indoor environment using fabricated prototypes of tag hardware. We show that our phase-based ranging performs similar to active receivers, providing median 1D ranging error  $< 1$  cm and median localization error also  $< 1$  cm. Benefiting from the large-scale link diversity our localization technique outperforms several state-of-the-art techniques that use active receivers.

## CCS CONCEPTS

• **Computer systems organization** → *Sensor networks*; • **Hardware** → *Networking hardware*.

## KEYWORDS

Backscatter communication, low-power communication, ranging, localization

Permission to make digital or hard copies of all or part of this work for personal or classroom use is granted without fee provided that copies are not made or distributed for profit or commercial advantage and that copies bear this notice and the full citation on the first page. Copyrights for components of this work owned by others than ACM must be honored. Abstracting with credit is permitted. To copy otherwise, or republish, to post on servers or to redistribute to lists, requires prior specific permission and/or a fee. Request permissions from [permissions@acm.org](mailto:permissions@acm.org).

*SenSys '21, November 15–17, 2021, Coimbra, Portugal*

© 2021 Association for Computing Machinery.

ACM ISBN 978-1-4503-9097-2/21/11...\$15.00

<https://doi.org/10.1145/3485730.3485950>

## ACM Reference Format:

Abeer Ahmad, Xiao Sha, Milutin Stanačević, Akshay Athalye, Petar M. Djurić, Samir R. Das. 2021. Enabling Passive Backscatter Tag Localization Without Active Receivers. In *The 19th ACM Conference on Embedded Networked Sensor Systems (SenSys '21), November 15–17, 2021, Coimbra, Portugal*. ACM, New York, NY, USA, 14 pages. <https://doi.org/10.1145/3485730.3485950>

## 1 INTRODUCTION

Backscattering implies a *passive* (radio-less) form of signal transmission achieved by reflecting an external RF signal. Such transmitters do not require an on-board radio which allows them to be battery-less, tiny and inexpensive. These properties make backscattering devices highly suited to the ubiquitous IoT vision, where all objects in our surrounding space carry such a device in the form of a tiny tag. However, almost all present-day backscattering systems, from the standard Radio Frequency Identification (RFID) [10] to other advanced technologies presented in the literature, rely on *active* radio-based devices *on the receive side of the backscatter link* (e.g., RFID reader). Such active receivers possess significant signal processing ability, and thus are power hungry and much more expensive in relation to the tags, thus posing a scalability challenge. A massive scale, ubiquitous deployment is always limited by number of these active devices that can be reasonably deployed.

One way to address the scalability issue is to enable passive reception of backscatter signals directly on the tags themselves, thus eliminating the need for separate active receivers. This enables direct tag-to-tag communications [15, 21, 32, 35, 40] and in turn multihop tag-to-tag networks [25, 35]. In this paradigm the external excitation signal to backscatter comes from an ambient source [21] or an intentionally deployed *exciter* [35, 43].<sup>1</sup> These research efforts have demonstrated the basic communication ability of passive tag-to-tag networks. However, for wide applicability, such tag networks must do more than basic send-receive functions. Many IoT applications need to go beyond mere identification of tagged objects (“things”) to forming ambient intelligence via understanding physical relationships and interactions between these objects. Accurate localization of the tags serves as the key enabler here. With more traditional active radio-based systems, the tag localization approaches gain significant support from the capabilities of the active receivers (e.g., RFID readers or analogous devices) to measure the strength, phase, angle of arrival or time of arrival of the received backscatter signal [5, 7, 31, 59]. Without such receivers, these approaches do not directly apply to passive tag-to-tag networks. Such tags must operate with the power harvested from the excitation signal (e.g., less than  $10 \mu\text{W}$ ) and thus must find a way to *measure received signal’s properties using passive techniques* such that accurate localization can be achieved while staying within the

<sup>1</sup>This distinction is not relevant for our work so long as there is enough signal power available for the tags to function.

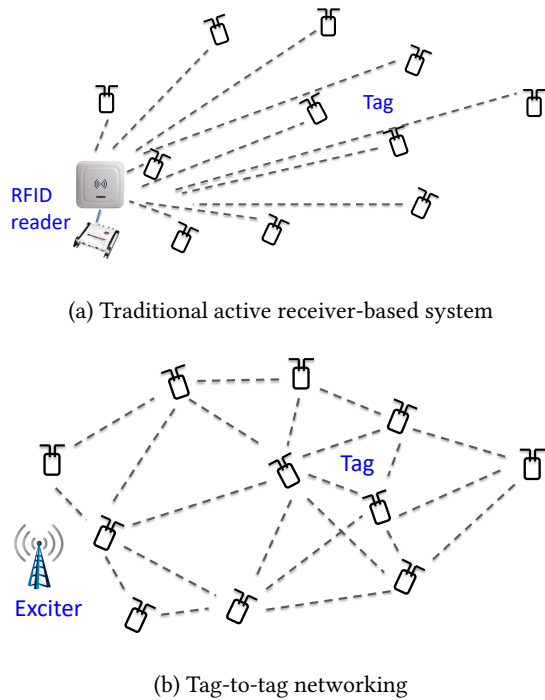


**Figure 1: Comparison between traditional active receiver-based system vs. tag-to-tag networking for the same tag deployment. For localization, the traditional system can only use measurements from the active receiver, perhaps from multiple vantage points for diversity (not shown). However, this diversity comes naturally in tag-to-tag networks .**

power budget. The overarching goal of this paper is to develop such a functionality.

## 1.1 Contributions

We make two related contributions. Our core contribution is *developing an accurate phase-based ranging technique between two backscattering passive tags*. We develop a technique to measure backscatter channel phase and amplitude between two communicating passive tags just like in an active receiver. We show that the phase measurements are accurate enough to provide a range estimate between two tags modulo half-wavelength (‘wrapped’ range). The accuracy of the wrapped range estimate (median error <1 cm) is comparable to active radio-based techniques.

Our second contribution is in *demonstrating that the channel measurement ability on tag-to-tag links also provides a significant localization advantage*. Traditional tag localization methods are limited only to measurements on tag to active receiver links. See Figure 1. The active receivers are ‘anchored’ with known locations. Since the number of active receivers is expected to be far smaller than the number of tags (active devices are larger, more expensive and power-hungry), tag-to-tag measurements provide a clear advantage of simply having measurements on many more links. For example, in active receiver systems, the maximum number of wireless links whose properties can be used to perform localization,

is  $O(nm)$ , where  $n$  is the number of tags and  $m$  is the number of anchor points (active receivers). Our technique, on the other hand, does not require active receivers. Replacing them by anchored passive tags, we can extract information from  $O((n+m)^2)$  links,<sup>2</sup> which could be significantly larger than  $O(nm)$ , given  $n \gg m$  in most cases of practical interest. When ranging estimates are formed on all such links, the localization benefits from the richness and diversity of many links. We show that tag-to-tag measurements are indeed able to provide much better localization accuracy when compared to an equivalent active receiver-based technique with no tag-to-tag measurements available.

## 1.2 Organization of The Paper

The rest of the paper is organized as follows. Section 2 introduces the fundamentals of passive tag-to-tag communication and summarizes related work. A mathematical modeling approach of the received backscatter signal is presented in Section 3. This leads to our proposed technique for tag-to-tag ranging, presented in Section 4. Section 5 describes the hardware architecture and implementation of the tag prototype. Section 6 presents an experimental evaluation of the phase based ranging method. Our technique for localization of passive tags based on this ranging is described in Section 7. Experimental evaluation of the localization method is done in Section 8 and Section 9 concludes the paper.

## 2 BACKGROUND AND RELATED WORK

Our work draws upon two technologies - passive tag-to-tag communication and backscatter tag localization.

### 2.1 Passive Tag-to-Tag Communication

Today, the most widespread practical embodiment of backscattering technology is in Radio Frequency Identification (RFID) systems [10]. In these systems, a passive backscattering tag communicates with an active device (RFID reader) which acts as the receiver of backscattered signals and also supplies the needed excitation signal. Over the past decade, research on backscatter systems has moved beyond the realm of RFID with researchers applying the underlying technology in the context of modern-day commodity wireless systems such as WiFi, Bluetooth and Zigbee. Broadly speaking, most of these efforts either attempt to generate signals compliant with the relevant standard using backscattering or piggyback backscatter communication onto a link comprising an active transmitter and receiver [6, 47, 56, 57]. *A common theme of all these studies is that, like RFID systems, an active receiver is still used to receive and process the backscatter signaling.*

To overcome the power and scalability challenges posed by a centralized active receiver, recent research efforts have proposed backscattering tag-to-tag networks wherein the passive tags communicate directly with each other without the need for an active receiver [15, 16, 21, 25, 32, 35, 36]. Compared to traditional RFID, the tags comprising such networks employ novel backscatter modulation and passive demodulation techniques enabling them to talk to each other [4, 40]. The excitation signal needed for the backscattering is provided either by ambient sources present in

<sup>2</sup>This can actually be done in a scalable fashion using only  $O((n+m))$  broadcasts. More in Section 5.3.

the environment [21] or by intentionally deployed, autonomous, zero-intelligence excitors [43]. The decentralized nature of the communication in conjunction with low power (passive) constituent devices makes this setup very well suited for large scalable deployments with high tag density. In such cases, tag location is of particular importance as it serves as an enabler for many IoT applications. While passive tag-to-tag links enable communication and networking between the widely deployed passive tags, the underlying technology presents a distinct challenge for tag localization that we will discuss momentarily (Section 2.3).

## 2.2 Localizing Backscattering Tags

Localization of backscatter-based tags has been a widely researched area since the advent of RFID systems [7, 18]. The basic methods work by first estimating the range between the tag and reader using the time-of-arrival (ToA), the phase and in some cases the RSSI of the backscatter signal [8, 11, 39, 45, 53]. Localization is done by ranging from multiple receiver locations followed by geometric trilateration or triangulation. Another approach to achieving spatial diversity necessary for triangulation is based on use of mobile readers or tags [22, 29, 30, 54]. In most practical NLoS scenarios these techniques are highly susceptible to multipath and noise. The phase of the backscatter signal is known to be much more robust to environmental degradation as opposed to RSSI making it a more popular metric for basing localization techniques [31, 41]. But receivers can only provide a wrapped version of the phase leading to an ambiguity in the range estimate of an integer number of carrier wavelengths [61]. In order to overcome this ambiguity, early efforts focused on measuring received signal phase at multiple frequencies [3, 20, 34, 58, 62]. These techniques are broadly referred to as Frequency Domain Phase Difference of Arrival (FD-PDOA). These techniques suffer from bandwidth limitations in the ISM bands in which conventional backscatter systems operate [19]. Approaches using UWB have been proposed to overcome this shortcoming [24].

Alternative to ranging techniques, fingerprinting methods aim to survey the environment using a set of reference tags placed at known locations [17, 48, 51]. Backscatter signals from a target tag are received contemporaneously with those from the reference tags. Localization works by quantifying the correlation between the received amplitude and/or phase of the target tag and those of all the reference tags [26, 41, 59]. While fingerprinting allows for a more variable environment, these methods are still susceptible to multipath [60].

More recently, techniques based on the radar principles of Synthetic Aperture (SA) and holographic methods have been used to enable accurate backscatter tag localization in practical multipath environments [27, 28, 48, 50, 52]. In these techniques, the backscatter signal phase is measured at multiple frequencies at different receiver antenna locations along a known trajectory. A similar concept is applicable when the receiver is stationary and the tag is mobile (inverse SA [33, 38]). The localization area is divided into a grid and a hologram is built denoting the likelihood of each grid point being the true location. These methods are becoming popular due to their high accuracy and robustness to multipath and noise. Regardless in all methods reviewed above active receivers are involved with multiple receive points.

## 2.3 Focus of This Work, Challenges and Benefits

This work brings backscatter tag localization, traditionally confined to the realm of active radio receivers, to envelope-detector based passive receivers. The primary challenge here is that because receivers are passive, they do not have the ability to readily provide the phase of the received backscatter signal. In all the aforementioned techniques, an active receiver performs IQ demodulation and carrier cancellation to determine parameters of the received signal. This requires an on-board radio absent in passive receivers. Furthermore, the tag-to-tag link can only exist in the presence of the external excitation signal. The kernel of a conventional backscattering system comprises only a single bidirectional channel between a passive tag and an active receiver which, in the context of localization, embodies the distance between the two. As opposed to this, the kernel of a passive tag-to-tag network comprises three channels, one bidirectional tag-to-tag channel and two unidirectional exciter to tag channels. Even if there was a way to measure backscatter signal at the passive receiver, they would not be reliable metrics for tag-to-tag localization as these parameters would be corrupted by the influence of the exciter to tag channels. The focus of this work is on overcoming these challenges to realize accurate localization in passive tag-to-tag networks.

To the best of our knowledge this is the first work to perform localization in passive tag-to-tag networks without the participation of an active receiver. Table 1 shows how the performance of our system (detailed in Section 8) compares with state-of-the-art active receiver-based systems. A common theme among all the localization methods reviewed above is that, irrespective of the underlying technique employed, the accuracy critically depends on receiver spatial diversity (captured by the factor ‘ $m$ ’ in Section 1.1). This can come in the form of active receivers at multiple locations, multiple antennas (separated by at least half wavelength) connected to the receiver or mobile receivers. None of these approaches is scalable in the context of a large-scale IoT setup. This is primarily due to the cost, complexity and power requirements involved in each of them. As Table 1 shows, in spite of not using any active receiver our proposed approach is comparable or better than most active receiver-based systems. The two cases that have exceptional performance use more specialized receivers or use a restricted setup (noted in the Table caption).

## 3 MATHEMATICAL MODELING OF RECEIVED BACKSCATTER

In this section we develop a model of the received signal for a tag-to-tag backscatter link. The model forms the basis of the ranging approach. Consider the basic tag-to-tag link shown in Figure 2, consisting of an exciter<sup>3</sup>  $E$  and two passive tags  $T_1$  and  $T_2$ . The distances between the exciter and each passive tag, and between the two passive tags are denoted as  $d_1$ ,  $d_2$ , and  $d_{12}$ , respectively. Both tags receive the excitation signal and have the ability to transmit using backscatter modulation and passively receive such transmissions from other tags in their vicinity. Consider a scenario where  $T_1$  backscatters. The signal received at  $T_2$  is a superposition of 1)

<sup>3</sup>Note, we are assuming an intentionally deployed exciter emitting a continuous wave (CW) signal. The analysis, however, can also extend to ambient RF signals.

Paper	Infrastructure needs		Area studied	Accuracy (median)
	No. of active Rx points	Reference tag density		
FaHO [52]	Single moving Rx (about 50 points in a 1 m)	N/A	1 m × 1 m	1–5 cm depending on scenario (ISM band)
RF-IDraw [49]	2 Rx each with 4 antennas	N/A	5 m × 6 m	4 cm in LoS case (ISM band)
3D Real-time [23]	4 Rx antennas	N/A	60 cm × 60 cm × 40 cm	3.5 cm (ISM band)
PinIt [48]	3 Rx points or mobile Rx at 30 cm/sec	≈ 6 tags/m <sup>2</sup>	6 m × 5 m × 2.2 m	11.2 cm (ISM band)
Tagoram [54] (Useful only for mobile tracking, not for static localization)	2 Rx antennas for known trajectory, 4 for unknown trajectory	N/A	130 cm linear track, 54 cm dia. circular track, arbitrary track in 10 cm × 10 cm	<1 cm known trajectory, 12.3 cm unknown trajectory (ISM band)
RFind [24]	3 Rx points capable of receiving ISM band and out of band frequencies (UWB)	N/A	10m × 12m	33 cm when using ISM band, 1 cm when using UWB
3D Landmarc [51]	4 Rx points	4 tags/m <sup>2</sup>	10m × 10m × 5 m	50 cm (ISM band)
SAIL [59]	3 to 4 Rx points	3 to 3.5 tags/m <sup>2</sup>	4.5m×5m, 2.4m×3m	35 cm in simulation, 90cm in experiments (ISM band)
This work	N/A	1.25 tags/m <sup>2</sup>	4m × 4m	<1 cm (ISM band)

**Table 1: Comparison with competitive backscatter tag localization studies. Our work here is the only study that does not use active receivers of any form, but still achieves very competitive performance. Of note, while Tagoram [54] and RFind [24] demonstrate superior performance in certain cases, they either operate in a restrictive setup (e.g., known trajectory for Tagoram) or need more relatively complex infrastructure (multiple Rx points with UWB support for RFind).**

the excitation signal and 2) the backscatter signal from  $T_1$ . The excitation signal is much stronger than the backscatter signal because  $d_2 < d_1 + d_{12}$  and because of the reflection loss from the backscatter. Unlike a conventional wireless link wherein the link incorporates one wireless channel (Tx to Rx), a single tag-to-tag link incorporates three wireless channels – exciter to backscattering tag ( $E$  to  $T_1$ ), exciter to receiving tag ( $E$  to  $T_2$ ) and between the two tags ( $T_1$  to  $T_2$ ).

The exciter transmits the signal  $S_E = A_E \cos(\omega t)$  where  $A_E$  is the amplitude and  $\omega = 2\pi f$ ,  $f$  being the carrier frequency. We denote the attenuations and phases of the respective exciter-to-tag and the tag-to-tag channels by  $\alpha_1, \alpha_2, \alpha_{12}$  and  $\theta_1, \theta_2, \theta_{12}$ . Then, the signals from the exciter received at  $T_1$  and  $T_2$  respectively are

$$S_{E \rightarrow T_1} = \alpha_1 A_E \cos(\omega t + \theta_1), \quad (3.1)$$

$$S_{E \rightarrow T_2} = \alpha_2 A_E \cos(\omega t + \theta_2). \quad (3.2)$$

The tags employ a passive envelope detector in the receiver, which provides voltage corresponding to the baseband envelope of the received signal. (More on the tag architecture is presented in Section 5.) The backscatter modulation is achieved by switching the antenna impedance between two states, viz. a conjugate matched state and a modulation state. The conjugate matched state is optimized for delivering maximum power to the tag chip, and the backscatter modulation state alters the antenna reflection coefficient  $\Gamma$  modulating the amplitude and phase of the reflected

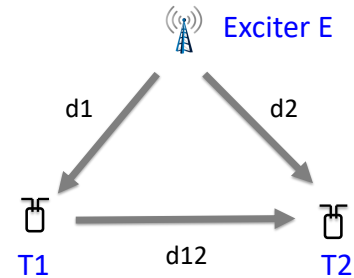


**Figure 2: Exciter  $E$  with two communicating tags  $T_1$  and  $T_2$ .**

signal. The strength of the backscattered signal is determined by the magnitude of the reflection coefficient  $|\Gamma| = \rho$  ( $0 \leq \rho \leq 1$ ) and the phase offset of the backscatter is determined by  $\angle \Gamma = \phi$ . These values are pre-determined.

We denote the detected voltage at the output of the envelope detectors of  $T_1$  and  $T_2$  when the other tag is not backscattering (i.e., the tag receives only excitation signal) as  $V_1$  and  $V_2$ , respectively. Recall that when one tag backscatters, the signal received at the other tag is a superposition of the received backscatter and the received excitation signal. When  $T_1$  is backscattering, the output at

the envelope detector of  $T_2$  is given by:

$$v_2 = V_2 + V_1 \alpha_{12} \cos(\theta_1 + \theta_{12} - \theta_2) - V_1 \alpha_{12} \rho \cos(\theta_1 + \theta_{12} - \theta_2 + \phi) \quad (3.3)$$

Similarly,  $v_1$  at the output of the envelope detector of  $T_1$  can be modeled when  $T_2$  is backscattering. See Appendix A for the complete derivation. The primary challenge in ranging is to estimate the two channel parameters  $\alpha_{12}$  and  $\theta_{12}$  based on this voltage  $v_2$ .

### 3.1 Approach

If one side of the backscatter link has an ‘active’ receiver, it can deploy well-known I-Q demodulation and can measure channel amplitude and phase directly. This ability has indeed empowered a variety of ranging techniques. However, a ‘passive’ receiver with an envelope detector can only track the baseband signal amplitude and cannot measure the carrier signal phase directly. A further complication here is that, the tags being radio-less, the carrier signal is externally supplied (by an exciter, e.g.) and not generated within one of the end point of the link. Thus, the parameters of the exciter-to-tag channel plays a role in our attempt to characterize the tag-to-tag backscatter channel (Equation 3.3), but directly estimating the tag-to-tag channel in isolation is not possible. We thus adopt an indirect approach described below.

The idea is based on multiple measurements of  $v_1$  and  $v_2$  with a range of different reflection coefficients  $\Gamma_i$ , represented by magnitude and phase pairs,  $\rho_i$  and  $\phi_i$ . The multiple reflection coefficients are enabled by a supportive tag architecture we discuss in Section 5. We show in Section 4 that such multiple measurements on both directions of the backscatter link ( $T_1$  to  $T_2$  and  $T_2$  to  $T_1$ ) provide information for estimating all the unknown parameters related to the exciter-to-tag channel in Equation 3.3 and estimate  $\alpha_{12}$  and  $\theta_{12}$ , the parameters of the tag-to-tag backscatter channel. Our prior work in this space [1, 2, 16, 36] provided some initial directions to this problem. However, these prior studies only developed a limited approach as their goals were different. This work, on the other hand, incorporates a general form of tag reflection coefficient and provides a simple linear equation-based solution approach that is doable on the tags. Further, the method is supported by extensive set of evaluations with applications to localization.

## 4 TAG-TO-TAG RANGE ESTIMATION

The estimation of tag-to-tag range (distance) is a two-step process: 1) estimating the backscatter channel parameters – amplitude and phase, and 2) estimating the ‘wrapped’ range (i.e., range modulo half-wavelength) by making use of these parameters. We discuss these steps in the following two subsections.

### 4.1 Channel Parameter Estimation

Let us denote the relative phase difference between the backscatter signal path and exciter signal path at  $T_2$  as  $\Theta_2 = \theta_1 + \theta_{12} - \theta_2$ . Substituting this into equation (3.3) and simplifying the envelope detector output at  $T_2$  becomes

$$v_2 = V_2 + V_1 \alpha_{12} [(1 - \rho \cos \phi) \cos \Theta_2 + \rho \sin \phi \sin \Theta_2]. \quad (4.4)$$

As explained before, now consider that each tag has the ability to backscatter by sequencing through  $N$  different reflection coefficients  $\Gamma_i$ ,  $i = 1 \dots N$ , each with known phase  $\phi_i$  and amplitude  $\rho_i$ . For each of these backscatters from  $T_1$  to  $T_2$ , we obtain  $N$  different voltages  $v_{2,i}$  at  $T_2$  (the new subscript  $i$  now refers to backscatters with different reflection coefficients). Thus, Equation 4.4 can be expanded into the following set of  $N$  equations for  $N$  such backscatters:

$$\underbrace{\begin{bmatrix} v_{2,1} & v_{2,2} & \dots & v_{2,N} \end{bmatrix}^T}_{\mathbf{v}_2} = \underbrace{\begin{bmatrix} 1 & 1 - \rho_{1,1} \cos(\phi_{1,1}) & \rho_{1,1} \sin(\phi_{1,1}) \\ 1 & 1 - \rho_{1,2} \cos(\phi_{1,2}) & \rho_{1,2} \sin(\phi_{1,2}) \\ \dots & \dots & \dots \\ 1 & 1 - \rho_{1,N} \cos(\phi_{1,N}) & \rho_{1,N} \sin(\phi_{1,N}) \end{bmatrix}}_{\mathbf{H}} \underbrace{\begin{bmatrix} V_2 \\ V_1 \alpha_{12} \cos(\Theta_2) \\ V_1 \alpha_{12} \sin(\Theta_2) \end{bmatrix}}_{\mathbf{x}_1} \quad (4.5)$$

This represents a set of linear equations of the form  $\mathbf{v}_2 = \mathbf{H} \mathbf{x}_1$ , with three unknowns  $V_2$ ,  $\Theta_2$  and  $\beta_2 = V_1 \alpha_{12}$ , and  $N$  measurements represented by the  $N$ -dimensional vector  $\mathbf{v}$ . The elements of  $\mathbf{H}$  in (4.5) are known quantities fixed by the tag hardware. They represent the amplitude and phase offset of the  $N$  reflection coefficients. By using  $N > 3$ , we obtain an overdetermined system of linear equations wherein the number of equations (measurements) is greater than the number of unknowns. This can be solved using the well-known least squares method to obtain estimates  $\widehat{V}_2$ ,  $\widehat{\Theta}_2$  and  $\widehat{\beta}_2$  as

$$\widehat{\mathbf{x}}_1 = (\mathbf{H}^T \mathbf{H})^{-1} \mathbf{H}^T \mathbf{v}_2 = \mathbf{W} \mathbf{v}_2, \quad (4.6)$$

where  $\mathbf{W} = (\mathbf{H}^T \mathbf{H})^{-1} \mathbf{H}^T$ .  $\widehat{V}_2$ ,  $\widehat{\Theta}_2$  and  $\widehat{\beta}_2$  are obtained from  $\widehat{\mathbf{x}}_1$ . If  $\widehat{\mathbf{x}}_1 = [\widehat{x}_1(1) \widehat{x}_1(2) \widehat{x}_1(3)]^T$ , following (4.5) we have:

$$\begin{aligned} \widehat{V}_2 &= \widehat{x}_1(1), \\ \widehat{\Theta}_2 &= \text{atan} \frac{\widehat{x}_1(3)}{\widehat{x}_1(2)}, \\ \widehat{\beta}_2 &= \sqrt{\widehat{x}_1(2)^2 + \widehat{x}_1(3)^2}. \end{aligned} \quad (4.7)$$

Note that  $\widehat{\Theta}_2$  is an estimate of wrapped phase  $\Theta_2$ . The above estimation has been developed for the case  $T_1$  backscattering to  $T_2$ . The same exercise can be repeated for the opposite direction,  $T_2$  backscattering to  $T_1$ . Thus, we can also obtain the estimates  $\widehat{V}_1$ ,  $\widehat{\Theta}_1$  and  $\widehat{\beta}_1$ , where  $\widehat{\beta}_1$  is an estimate of  $V_2 \alpha_{12}$  by the same procedure. Using both sets of estimates, the backscatter channel parameters  $\alpha_{12}$  and  $\theta_{12}$  are estimated as

$$\widehat{\alpha}_{12} = \frac{1}{2} \left( \frac{\widehat{\beta}_1}{\widehat{V}_2} + \frac{\widehat{\beta}_2}{\widehat{V}_1} \right) \quad (4.8)$$

and

$$\widehat{\theta}_{12} = \left( \frac{\widehat{\Theta}_1 + \widehat{\Theta}_2}{2} \right) \bmod \pi. \quad (4.9)$$

Note that  $\widehat{\theta}_{12}$  provides estimate of  $(\theta_{12}) \bmod \pi$ .

For the selection of the reflection coefficients  $\Gamma_i$ , we choose to maximize the amplitudes  $\rho_i$  in order to improve signal-to-noise ratio. The phases  $\phi_i$  are selected to be equidistant in a range from 0 to  $2\pi$ .

Procedurally, the channel parameter estimates can be obtained as follows. Every pair of tags in the tag network that is able to communicate in both directions, performs a sequence of  $N$  backscatters in each direction using the  $N$  reflection coefficients (called *multiphase probing* or MPP [36]). This provides the measurement vectors  $\mathbf{v}_1$  and  $\mathbf{v}_2$  at the output of the envelope detector of  $T_1$  and  $T_2$ , respectively. Matrix  $\mathbf{W}$  is precomputed based on the selected reflection coefficients  $\Gamma_i$  and stored on tag. Estimation of  $\mathbf{x}_1$  and  $\mathbf{x}_2$  at each tag is then obtained using vector-matrix multiplication. From estimated values of  $\mathbf{x}_1$  and  $\mathbf{x}_2$ , channel attenuation and phase,  $\hat{\alpha}_{12}$  and  $\hat{\theta}_{12}$ , are obtained. Related protocol issues are discussed in Section 5.3.

Note that the exciter-to-tag channel parameters are eliminated from consideration by the above method. Although, we used a direct path model of the exciter-to-tag channel in the derivation, the same model applies in the case of the multipath in this channel, as the exciter is a single-frequency CW signal. Therefore, the proposed technique cancels the effect of that multipath in exciter-to-tag channel. This will be experimentally demonstrated in Section 6.

## 4.2 Range Estimation

In principle, the channel phase and attenuation parameters estimated in the previous subsection can be directly used for estimating the distance between the tag pair in question. We proceed with the phase-based distance estimation, due to sensitivity of the amplitude-based estimation on antenna orientation and multipath propagation [37]. The phase-based estimation while more reliable, suffers from an ambiguity due to the phase wraparound every  $2\pi$ :

$$\theta_{12} = \frac{2\pi d_{12}}{\lambda} \Big|_{\text{mod } 2\pi} \quad (4.10)$$

As we estimate  $(\theta_{12}) \bmod \pi$  (Equation 4.9), the estimate of the tag-to-tag distance  $d_{12}$  is

$$\hat{d}_{12} = \frac{\lambda}{2\pi} \hat{\theta}_{12} + k\lambda/2, \quad (4.11)$$

where  $k$  is an unknown non-negative integer which causes the ambiguity in distance estimation. While we can estimate only the ‘wrapped’ range, the localization method that we use (Section 7) will be able to perform the unwrapping for correct localization.

## 5 TAG ARCHITECTURE AND IMPLEMENTATION

To implement the proposed tag-to-tag range estimation, the passive backscatter tag should have three important components: 1) a *multiphase modulator* that implements backscattering using a range of different reflection coefficients (Section 3.1 and 4.1), 2) an envelope detector-based demodulator followed by 3) an analog-to-digital converter (ADC). The estimates of the tag-to-tag channel amplitude and phase are then computed in digital domain as described in Section 4.1. For the evaluation of the proposed method and data collection, we implement a printed-circuit board (PCB) version of the tag with commodity discrete components. The PCB has a USB interface to PC for data transfer. We also have interface to SD memory card for autonomous data collection (Figures 3 and 4). Such a discrete component-based set up allows for experimental convenience as individual tag data can be directly collected and

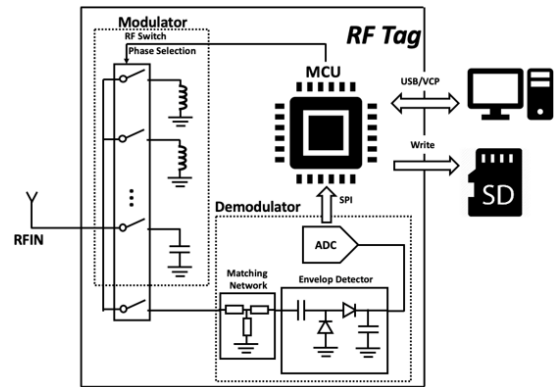


Figure 3: Block diagram of backscatter-based tag-to-tag PCB design.

analyzed. However, the discrete component-based design does not run on harvested power. Thus, we separately demonstrate how an on-chip ASIC version of the tag can be designed that is able to run from harvested RF energy alone.

## 5.1 Discrete Component-based Implementation

Figure 3 shows the block diagram of the discrete component-based tag implementation that we use for our experimental validation. The image of the front and back side of the PCB is shown in Figure 4. A dipole antenna is used to achieve an omnidirectional radiation pattern while also being simple to build for ubiquitous tagging.

The backscatter modulator of the tag is implemented using a 10-channel multi-port RF switch (SKY13404) [42]. Recall from Section 4.1 that our approach to estimate tag-to-tag channel parameters is based on the ability of the tag to introduce multiple pre-determined phase offsets in the reflected signal (multi-phase probing or MPP). As shown in Figure 3, the backscatter modulator allows for switching the tag’s reflection coefficient between multiple complex values  $\Gamma_i$ , each of which is characterized by magnitude  $\rho_i$  which determines what fraction of the incident signal is reflected and a phase  $\phi_i$  which determines the introduced phase offset. We have chosen to use 8 different reflection coefficients,  $N = 8$ , with each of these switch ports terminated with appropriate inductor and capacitor values. The values are chosen to have magnitudes of the reflection coefficient close to 1 and the phases almost equidistantly placed in the range from 0 to  $2\pi$ . The RF switch is controlled by a microcontroller unit (MCU). We have used Arm-based STM32F205RET6 [44].

One port of the RF switch is connected to a passive demodulator preceded by a T-type matching network. The matching network maximizes the output voltage of the demodulator by providing an input impedance of  $200 \Omega$  at input power of  $-17$  dBm. The demodulator consists of an envelope detector, implemented as a two-stage Dickson rectifier. Schottky diodes, SMS7630 [13], are used as the rectifying elements. The envelope detector is followed by an amplifier and low-pass filter with a cut-off frequency of 100 kHz. While a conventional RFID tag would have a comparator after the envelope

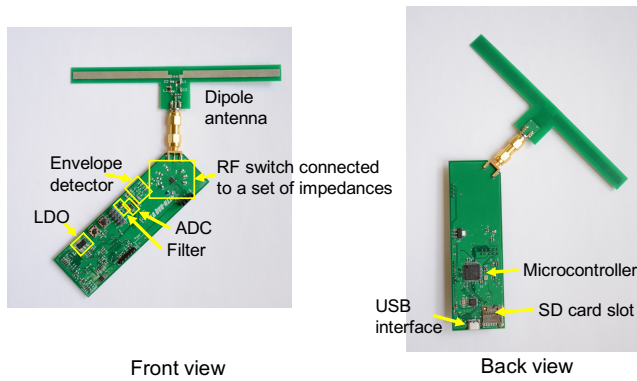


Figure 4: Tag hardware (front and back).

detector (as the tag is only used for the communication) in our discrete implementation, the baseband signal is digitized by a 16-bit 1Mbps ADC, ADS8860 [14]. The MCU collects digital data from the ADC via SPI communication. For the experimental study, data can be written into a on-board micro SD card or transferred to PC using USB connector.

While in an optimized ASIC implementation the tag would operate using harvested RF power alone (next subsection), the discrete component-based implementation here needs external power to operate, as the discrete components such as the MCU or ADC cannot be power-optimized. The board described here operates from a single 3.3 V voltage regulator. The input voltage to the regulator is either provided through USB connection or a battery for autonomous operation.

## 5.2 On-Chip Tag Architecture and Power Budget

To miniaturize the tag and also to minimize the power consumption, the tag must be implemented in application specific integrated circuit (ASIC). We have designed some of the basic functionalities of the tag in ASIC already and they have been reported elsewhere [12, 16]. For the sake of completeness, we briefly describe the ASIC design below and also discuss the power consumption.

The on-chip tag architecture is shown in Figure 5. It comprises the modulator and demodulator, power harvester with power management and an energy storage element, along with communication control and computational logic. The tag also integrates volatile and non-volatile memory for data storage. The implementation of the energy harvester along with the power management circuitry, modulator and demodulator in 65 nm CMOS technology is described in [12, 16].

The power harvester converts incident RF energy at the antenna to a DC supply voltage for the operation of the tag. The power management strategy determines the operating regime of the harvester based on the input power level. The power sensitivity of the tag is  $-34.4$  dBm ( $0.36 \mu\text{W}$ ) [12]. At this input power level, the tag harvests RF energy, stores it on a supercapacitor and is able periodically performs tasks like communication and channel sensing after enough energy is harvested. In the range of the input powers from  $-25$  dBm

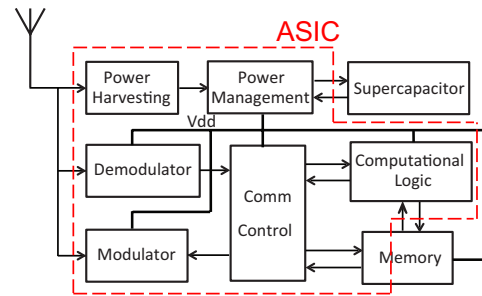


Figure 5: On-chip architecture of the proposed tag.

up to  $-5$  dBm, the harvesting circuit can instantaneously generate the supply voltage for the operation of the tag. Any excess energy is stored in the supercapacitor. The power efficiency of the energy harvester itself is higher than 50% over this range [12].

The multi-phase probing modulator comprises a multi-port RF switch and control logic. For data rates up to 10 kbps, the power consumption of a discrete multi-channel RF switch is about 150 nW [46]. When we implement on-chip, due to the lower internal capacitance, the power consumption is expected to reduce to 10s of nW. The demodulator, however, consumes more power. In a discrete implementation of the tag (Section 5.1), the demodulator samples the baseband signal after the envelope detection with 16-bit resolution. The time-waveform of the baseband signal in the tag-to-tag link is in a form of an ASK modulated signal with a low modulation index [15]. By inserting the amplifier with integrated high pass filtering, DC level of the signal is eliminated and the filtered baseband signal can be sampled with 8-bit ADC in order to achieve similar resolution [16]. We have demonstrated that such a tailored demodulator can perform the channel sensing with a modulation index as low as 2.5% [16] with power consumption in the order of 100 nW, albeit with a somewhat lower bit rate, 4 kbps. The demodulator functions as a wake up circuit when ADC is reconfigured to a 1-bit resolution, which enables circuit to meet more stringent power consumption constraint in this mode of operation. Put together, the proposed ASIC implementation of the modulator and demodulator along with 8-bit ADC designed in the 65 nm CMOS fabrication technology consumes power comfortably lower than  $1 \mu\text{W}$ .

The tag also includes computational logic in order to perform channel phase estimation, along with the on-chip volatile memory and off-chip non-volatile memory for data storage. Although we have not directly investigated the IC design for this, the power estimates can be obtained based on the required computational tasks and the data routing functionality needed. For channel phase estimation, computational tasks according to (4.6)–(4.8) need to be performed following baseband signal digitization. The matrix  $\mathbf{W}$  has a dimension of  $3 \times 8$ , so the matrix-vector multiplication (4.6) is not computationally intensive. Recall that the matrix  $\mathbf{W}$  itself is precomputed. For the power consumption related to all computational steps, it is important to note that the operating frequency does not exceed 1 MHz, as the projected data rate in tag-to-tag communication is max 10 kbps (see our prior work using an earlier version of the tag [15, 35]). Based on the above, a custom microprocessor with ARM Cortex M0 and 3 kB SRAM that consumes

90 nW [9] is sufficient for the estimation of tag-to-tag channel parameters. Accounting for a certain additional amount for various housekeeping functions and routing functionality, the power limit on the computation and control logic should not exceed  $1 \mu\text{W}$ .

Thus, after accounting for all the building blocks of the tag, the total power budget can be as low as  $2 \mu\text{W}$ . Assuming that the efficiency of the power harvesting is on the order of 30-40% (including impedance matching), the incident RF power at tag that corresponds to this power budget is about -22 dBm. In the protocol description that follows, we assume that the excitation power is available in a continuous fashion at this level. As noted above, as energy can be stored in the supercapacitor lower power operation is possible, since the tags only need to function intermittently for a vast majority of applications. However, this will require a synergistic operation of the higher layer functions with the tag power management. This is a topic of our future work.

### 5.3 Protocol to Support Channel Parameter Estimation

In this section, we briefly describe the necessary protocol aspects of channel parameter estimation.

*Encoding Scheme.* The data encoding scheme used must allow for efficient power harvesting and be amenable to decoding without IQ demodulation while relying on a simple switch based backscatter modulator. Encoding schemes for passive wireless systems have been analyzed in [55]. Based on these criteria and borrowing relevant concepts from the Gen 2 standard, we use a combination of pulse interval and Miller encoding in our system. Symbols (Data-0, Data-1, calibration or other) are encoded by the interval between signal transitions. This also ensures that our link can handle phase shift (causing bit-flipping) in the demodulated signal. Decoding of symbols is done by counting the number of clock cycles between successive edges in the demodulated signal.

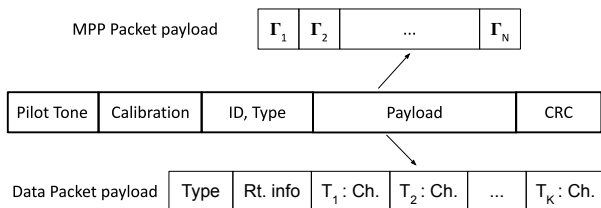


**Figure 6: Packet format. MPP payload contains backscatter signals with  $N$  reflection coefficients and Data payload consists of channel measures with  $K$  neighboring tags.**

*Packet Format.* In the tag network, tags can transmit two kinds of packets, viz. (a) multiphase probing (MPP) packet for channel estimation (Section 4.1) and (b) data packet. The packet structure for our network is shown in Figure 6. It starts with a pilot tone consisting of a fixed number of pulse transitions at the lowest rate supported by the network. This is done to minimize the energy consumption of the wake-up circuit on the receiving tags. This is

followed by a calibration sequence which allows the receiving tags to calibrate the number of clock cycles between edges of the different data symbols. The packet header includes a tag ID and a packet designator which indicates whether it is a MPP or data. The data packet payload depends on the type of the data packet. For example, as shown in the figure, it may consist of a list of all neighbouring tags that the transmitting tag sees along with the corresponding channel parameters measured for each tag ( $x$  vector in Equation 4.5). Alternatively, it may include relayed information from remote tags (Section 7.2) along with routing related information, such as the final destination and any other protocol or forwarding related information. Routing control packets are also treated as data packets with suitable Type designation and necessary fields. The packet payload is followed by a CRC for data integrity.

*Multiphase Probing (MPP).* For channel measurements, a transmitting tag cycles through all  $N$  reflection coefficients in a predetermined sequence backscattering the incident RF signal. In an earlier work, we used such probing for a different purpose [36]. The dwell time at each reflection coefficient is about  $100 \mu\text{s}$ . We assume that the channel/environment remains unchanged during each MPP cycle. The MPP provides the opportunity for each receiving tag to measure its channel w.r.t the transmitting tag (Section 4.1). Subsequently, each tag broadcasts the complete set of measured values (one set of measurements for each neighboring tag) for all the neighboring tags to listen to. All these can be achieved by  $O(n)$  broadcast operations for a total  $n$  tags in the network.

The collision resolution follows traditional CSMA principles as described in our earlier work with similar tags [35]. Similar ideas are also reported in [21, 25]. The application we consider (localization) the speed of operations is not critical with the assumption that the tag network is largely stationary and rapid movements are infrequent. Thus, MPP broadcasts followed by data broadcasts at suitably spaced intervals will enable all tags in the network acquire channel measurements data between itself and its neighboring tags. This can be repeated periodically for robustness and/or to capture any changes.

## 6 EXPERIMENTAL EVALUATION

In this section we describe the experimental setup and results evaluating the performance of the proposed tag-to-tag range estimation technique. The evaluation only considers channel measurements at both ends of a tag-to-tag-link. It does not use tag-to-tag communications. Tag-to-tag communications have been separately demonstrated in [35] using an earlier version of the same tag.

### 6.1 Experimental Setup

In all performed experiments, we use a continuous wave (CW) RF signal generator as the exciter with transmit power varying between 9–13 dBm and operating at frequency 915 MHz. A circularly polarized antenna with gain 6dBiC is used. The exciter provides the necessary RF signal to backscatter.

Two tags are set up on a rail (Figure 7) so that the inter-tag distance can be adjusted easily. The rail is positioned about 1.5 m away from the exciter antenna. For each inter-tag distance we measure, each tag performs a full MPP cycle with the other tag collecting the digitized baseband signal. This determines one measurement

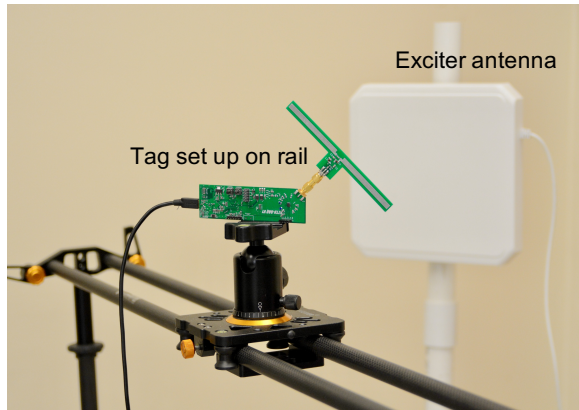


Figure 7: Experimental setup (only one tag is shown)

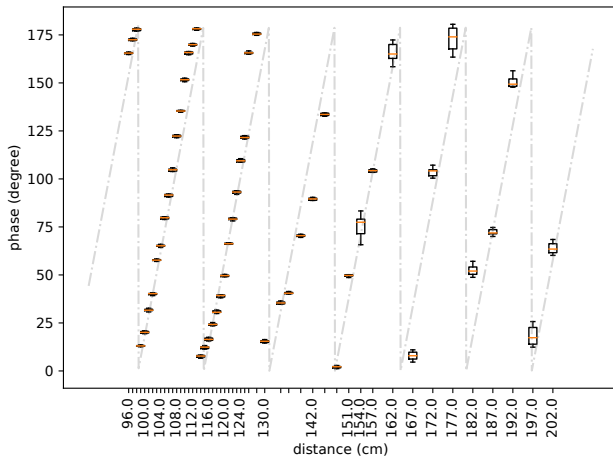


Figure 8: Measured phase on tag-to-tag link for various inter-tag distances. The dotted line shows the actual phase.

cycle and provides the necessary data for estimating the channel phase and range (Section 4). The data set is collected and analyzed on a PC. The input power at the tags for the experiments are in the range of -15 dBm to -18 dBm. The reported experiments are done in a laboratory environment with significant scopes for multipath. Parts of the experiments have also been repeated in the living room of an apartment. This latter set of experiments exhibits similar characteristics and accuracy and is thus not reported separately.

### 6.2 Evaluation of Range Estimation

In Figure 8, we show the estimated channel phase for various tag-to-tag distances upto about 2 m following the procedure outlined in Section 4. For each distance, measurements are repeated 100 times, sometimes with different exciter powers. Since slight variations are noted in the estimated phase at the same tag positions, the resulting distributions are captured using box plots. These variations are likely due to channel noise and electronic noise. The variations are very small – within a few degrees upto about 1.5 m and going

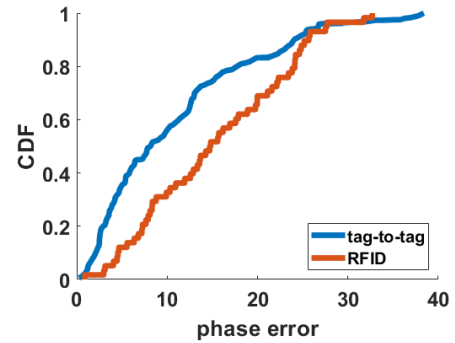


Figure 9: CDF of median phase estimation errors across all distances.

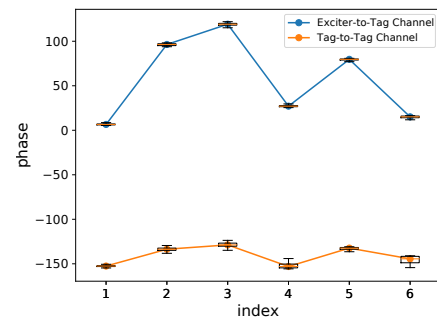


Figure 10: Impact of changes in exciter to tag channels

up to about 20° at the higher end. Given the wavelength (33 cm), even a 20° error results in <2 cm distance estimation error. Larger variations for longer links are expected due to increased channel noise. Overall, the estimated phase tracks the actual phase (modulo  $\pi$ ) very well. The systematic deviations that are noted (deviation of the median of measured phase from the actual phase) are likely due to multipath effects that are not directly modeled in our technique. This is typically within 10°, equivalent to <1 cm range estimation error. Generally, for shorter links the systematic errors due to the multipath effects dominate. For longer links, the multipath errors and the errors due to channel noise and electronic noise are similar.

We also performed a similar set of measurements in the same environment with an RFID reader (Speedway Revolution R20) and a Gen2 tag by measuring the channel phase on the reader for different reader-tag distances. This provides a baseline for channel estimation using an active receiver to tag.

Figure 9 captures the CDF of the phase estimation error of the measurements reported in Figure 8. We also add a similar plot corresponding to the RFID reader-based baseline, which shows a slightly higher error. This clearly demonstrates that accurate channel measurements are possible using entirely passive techniques on tags operating on harvested power.

Finally, it is instructive to discuss the impact of excitation powers and obtainable ranges. We have seen very little sensitivity of phase estimation error to excitation power. However, the tag-to-tag

range becomes limited with lower available power, falling down to about 1.5 m with 9 dBm. While the measurements are performed up to  $\approx 2$  m tag-to-tag range, higher ranges are certainly possible with higher excitation power (higher than 13 dBm) and/or lower thermal noise and ripple voltage levels at the tag (possible in the ASIC implementation). The latter ultimately impacts the sensitivity of the tag. The tag-to-tag range is impacted by available excitation powers at both transmit and receive sides in the following ways. Higher power on transmit side simply backscatters more power. Higher power on receive side (up to a limit) generally improves the sensitivity due to certain non-linearities present in the demodulator circuit. Note that we operated at modest excitation power levels. Determining the maximum possible operating range and its relationship with the hardware characteristics and excitation power levels is beyond the scope of this paper. A significantly higher range than is demonstrated here is indeed possible with right parameters. See [15], for example, for our analysis of possible tag-to-tag ranges for use in communications.

### 6.3 Invariance of Tag-to-tag Channel Estimation

The modeling approach in Section 4 removes the impact of the exciter to tag channels from the estimation. This is important as the exciter is expected to be further away from the tags and thus these channels are more prone to multipath and other adverse impacts. To demonstrate that our approach effectively removes any influence of the exciter to tag channels, we repeat similar experiments as above, but now varying the exciter locations arbitrarily with the tag locations fixed. This impacts the exciter to tag channels significantly. Figure 10 captures 6 such sets of experiments for 6 different exciter locations. Note the significant changes in the exciter to tag channels (the reported phase estimates  $\theta_1 - \theta_{12} + \theta_2$ ). The changes in the tag-to-tag channel ( $\theta_{12}$ ) are much less pronounced and similar to what we have seen before.

## 7 LOCALIZATION OF PASSIVE TAGS

The power of our localization method lies not in the actual computational technique used, but in the fact that *it is able to leverage large number of tag-to-tag links*. This is particularly useful in densely tagged environment. Tag-to-tag links are possible in an otherwise equivalent active radio based systems (e.g., RFID). In the latter case the links that can be measured are only between a tag and the active radio (e.g., RFID reader or similar device). The active radios are clearly much less numerous than passive tags in any setup and this limits the number of links that can be utilized.

We assume that a subset of the devices have known locations and every other device is localized w.r.t. them. Again, in a more traditional active radio-based case, these pre-localized devices are the active radios; they are typically externally powered and anchored. Existing active radio-based localization and tracking literature use this assumption (Section 2). To match this assumption in the tag-to-tag case, we assume that *there is a small set of ‘anchor’ tags with known locations*. The rest of the tags are to be localized w.r.t. these anchor tags. Our goal is to demonstrate that the rich diversity of tag-to-tag links brings significant benefits in terms of accuracy.

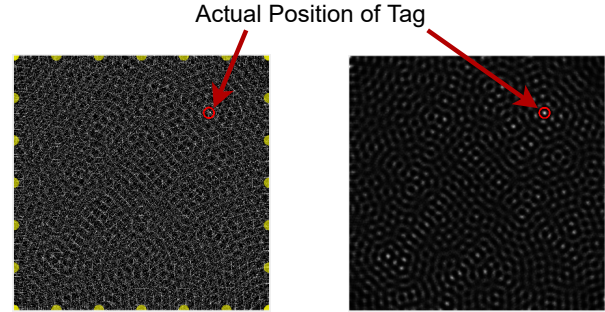


**Figure 11: (a) Concentric circles centered around the anchors (yellow dots) showing lines of equal phase and thus possible locations of the target tag  $T$ . (b) Hologram showing the distribution of the likelihood with the peak occurring close to the target location.**

The localization takes advantage of the ‘wrapped’ range estimation (Section 4). The wrapping issue is addressed using a likelihood based technique described in the following. Note that we limit the problem here to two dimensions for simplicity, but the techniques we use are general and can also apply to three dimensions.

### 7.1 Iterative Likelihood-based Localization

Recall from Equation 4.9 that we have a  $k\lambda/2$  ambiguity in the distance estimate, where  $k$  is a non-negative integer (4.11). Consider a specific tag  $T$  to be localized with its distance estimates from a set of anchors (4.11). The  $k\lambda/2$  ambiguity in the distance estimate results in concentric circles that are  $\lambda/2$  apart centered around these anchor tags. These circles represent possible locations of tag  $T$  (see Figure 11). We note that the actual distance estimate is obtained from noisy measurements (Section 6), and therefore, it is simply a random variable. We use the concentric circles around the anchors as a guide to generate a function representing the likelihood of the tag  $T$  being present at any of the points of the area being considered. This function is created by treating the concentric circles as an image and employing a Gaussian blur, i.e., convolving the image with a Gaussian function with zero mean and standard deviation  $\sigma$ , where  $\sigma$  is obtained from prior measurement studies (Section 6). With the blurring we create a “likelihood function” as if it was obtained using noisy measurements. The point with the largest value in the blurred image represents the peak of the function (the highest likelihood). This is the most likely location of tag  $T$ .

We introduce a measure of confidence in this location estimate by considering other peaks of the function. If the second highest peak is close enough in value to the highest peak, this suggests a lack of confidence in the estimate. In this case, the tag is not immediately localized. Instead, the method is iterated multiple times, by treating the already localized tags as new anchors. This enables localization of the tags that could not be localized in the previous iterations. This is repeated until no additional tags can be localized. In our experiments (next section) 3–5 iterations were usually sufficient.

Mathematically, each iteration of the procedure is as follows. Let  $(x_i, y_i)$  be the coordinates of the  $i$ -th anchor, and  $(x_j, y_j)$  the coordinates of the  $j$ -th tag. Further, assume that we partition the space of interest into small cells where the center of each cell has

coordinates  $(x_r, y_c)$ . Next, for every triplet of indices  $(i, j, k)$  we define a matrix  $M^{[i,j]}[k]$  with elements  $M_{r,c}^{[i,j]}[k]$  given by

$$M_{r,c}^{[i,j]}[k] = \begin{cases} 1, & \text{if } |(x_r - x_i)^2 + (y_c - y_i)^2 - (\tilde{d}_{ij} + k\lambda)^2| < \delta \\ 0, & \text{otherwise,} \end{cases}$$

where  $\delta$  is some small predefined threshold. Thus, this matrix is composed of zero-one elements, where the elements with values one correspond to candidate locations of the  $j$ -th tag (for a given anchor  $i$  and value  $k$ ). Then for the  $j$ -th tag we construct a matrix  $H^{[j]}$ , which is obtained by aggregating the values of all the anchor matrices and all  $k$ 's, i.e.,

$$H_{r,c}^{[j]} = \sum_{\langle i \rangle} \sum_{\langle k \rangle} M_{r,c}^{[i,j]}[k]. \quad (7.12)$$

Finally, for the  $j$ -th tag we compute a matrix  $B^{[j]}$ , which approximates the likelihood of the tag's location and is used for processing in our iterative scheme. We define its elements by

$$B_{r,c}^{[j]} = \sum_{\langle n \rangle} \sum_{\langle m \rangle} G_{n,m} H_{n-r, m-c}^{[j]}, \quad (7.13)$$

where  $G$  is a filter introducing Gaussian-blur with zero mean and standard deviation  $\sigma$  to the matrix  $H^{[j]}$ . The matrix  $B^{[j]}$  contains the information about the location of the  $j$ th tag. The peak value of this matrix determines the likely location of the tag.

## 7.2 Protocol Considerations

Currently, the entire localization method is assumed to be done centrally while the channel measurements are distributed. As mentioned in Section 5.3, tags estimate the vector  $\mathbf{x}$  for all neighboring tags. These data set is communicated to a central location using multihop routing. Depending on the scale of the tag network one or multiple gateway or sink nodes can be used for data collection. Each tag simply routes data towards the sink closest to itself. The gateway nodes are similar to tags, but with an external wired or wireless connectivity. One or more anchor tags can play this role. Note here that some sort of external network connectivity is needed anyway to enable any application.

Multihop routing with sinks for data collection is a very mature topic and have been abundantly described in sensor network literature. A range of different techniques can be used. For brevity we do not repeat the possible techniques here. Depending on the application needs, the data collection can be repeated periodically. Optimization such as relaying only differences instead of actual values are expected to reduce the network burden. From a protocol perspective, a tag operates in one of three modes: *LISTEN* wherein the tag listens to communication from neighbors, *MPP* where the tag broadcasts MPP packets for channel estimation and *DATA COMM* when the tag transmits data to its neighbors. The data here could be its own measurements, or measurement data from remote tags en route to the sink. A tag alternates between MPP and DATA COMM with intervening times spent in LISTEN.

Depending on the network size, number of sinks and density of tags (that determines the interference environment), it is expected that there is a latency between when the channel measurements are performed and when the locations are computed. This not unusual for a sensor network environment that is dependent on multihop data collection.

Note that once all tags are localized via the proposed approach, incremental location changes in a small number of tags can be computed entirely locally. To see this, assume only one tag  $T$  moves slightly.  $T$  can measure the channel phase  $\theta$  w.r.t its neighbors. Assuming that the movement is very small relative to the wavelength,  $k$  in Equation 4.11 will either remain unchanged or will change only by 1. This can be estimated accurately by noting the change in  $\theta$  w.r.t all neighboring tags. One  $k$  is known, it is straightforward to re-localize  $T$  via multilateration.

## 8 EVALUATING LOCALIZATION PERFORMANCE

The localization performance is evaluated using a synthetic data set generated utilizing the data gathered for the tag-pair measurements described in Section 6 at different distances. Here, we imagine that a number of passive tags to be localized are distributed randomly in a  $4\text{ m} \times 4\text{ m}$  area. We assume that that the measured channel parameters between a tag pair located at a given distance is statistically similar to the measurement obtained for a similar distance in the data set collected in Section 6. In other words, any error would be statistically similar to the previous measurements. This assumption lets us make a large number of evaluations with different parameter settings without having to set up an actual tag network. Note that even though this is a trace-driven analysis, the measurements errors and noises are correctly captured as the data is coming from actual measurements. But it is assumed that no additional errors are possible due to any data communications error. This assumption is reasonable as, while packet losses are possible in the tag-to-tag network, any information loss is unlikely due to the significant amount of redundancy.

We assume the presence of a number of pre-localized anchor tags, which are otherwise identical to the regular tags except that their locations are known in advance. Given that well-distributed anchors are expected to provide the best localization performance, we assume that the anchors are set up uniformly on the perimeter of the area being considered (Figure 11). We vary the number of anchors and regular tags. Anchors being set up on the perimeter is not a requirement. All we have to be mindful of is that the performance is sensitive to each tag being able to reach multiple anchors. Deployment along the perimeter is typically convenient for most applications.

Figure 12 shows the CDF of location error with the iterative method described in Section 7. In order to demonstrate the power of tag-to-tag measurements, we also show a 'baseline' evaluation of the same localization technique where tag-to-tag measurements are not available and only anchor-to-tag measurements are available. This 'simulates' the base case, where anchors are active receivers (e.g., RFID readers) capable of doing phase measurements to tags. Comparison with such a baseline demonstrates the potential of tag-to-tag measurements – they clearly provide superior localization performance (Figure 12). Our experiments show (only part of the data presented here for brevity) that once sufficient number of anchors are present, the accuracy of the proposed technique is quite stable and largely independent of number of anchors and tags. The median accuracy is  $< 0.8\text{ cm}$ , slightly lower than the range estimation error (Section 6). The 90-percentile accuracy is also very

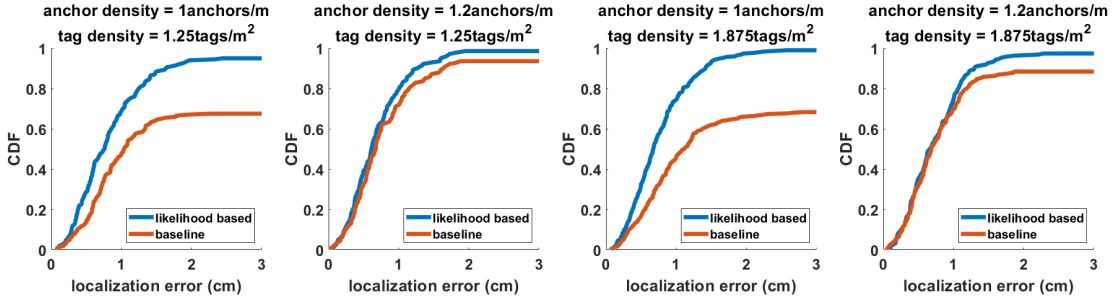


**Figure 12: CDF of localization error for various anchor and tag densities. The proposed likelihood-based method is compared with a ‘baseline’ where tag to tag measurements are not available.**

good, <2 cm. The baseline method performs poorly with smaller number of anchors. Even with larger number of anchors, its 90-percentile performance is poor while the median is comparable to the likelihood-based technique. This is expected, as the baseline method is based on only anchor-to-tag measurements.

At this point it is instructive to draw comparison with the related backscatter tag localization techniques in literature (Table 1 presented earlier in the paper). Each of these techniques need multiple active receivers or mobile receivers. Some of them also need additional reference tags (similar to anchor tags). Our proposed approach provides better accuracy (sub-centimeter) w.r.t. most of these approaches. The two techniques that are capable of comparable accuracy (Tagoram [54] and RFind [24]) either use a restrictive set up (e.g., fixed trajectory) or significantly complex Tx-Rx technology (e.g., UWB) that is even harder to scale.

## 9 CONCLUSIONS

This is the first work that provides a robust methodology to localize passive backscatter tags without requiring active radio receivers. This provides a tremendous scalability advantage. The method is based on ranging on tag-to-tag links using a novel passive channel estimation technique. The estimation technique is supported analytically and is shown to eliminate any impact of extraneous factors such as exciter to tag channels. Prototyping experiments with our developed tags show excellent ranging performance – below 1 cm median error, if the phase wraparound effect every half wavelength is ignored. We extend this technique to localization in a tag-to-tag network that benefits from the ability to measure on every tag-to-tag link. Overall, this provides competitive or superior performance to the tag localization techniques available in literature, while the latter techniques depend on multiple active receivers or antennas for similar localization performance.

## APPENDIX

### A Mathematical Modeling of Backscatter Signal

As shown in Figure 2, the excitation signals received at the two tags when the other tag is not reflecting are  $V_1 \cos(\omega t + \theta_1)$  and  $V_2 \cos(\omega t + \theta_2)$ . We observe the signal at tag  $T_2$  when tag  $T_1$  reflects with a reflection coefficient  $\Gamma_{1,k}$ , which has amplitude  $\rho_{1,k} = |\Gamma_{1,k}|$  and phase  $\phi_{1,k} = \angle \Gamma_{1,k}$ . The reflection coefficient  $\Gamma_{1,k}$  is set by the

impedance connected to the  $k$ -th port of the RF switch in the modulator of tag  $T_1$ . Tag  $T_2$  receives two signals, the backscatter signal from tag  $T_1$  and the excitation signal. These two signals are:

$$\begin{aligned} v_{T_1 \rightarrow T_2} &= V_1 |1 - \Gamma_{1,k}| \alpha_{12} \cos(\omega t + \theta_1 + \angle(1 - \Gamma_{1,k}) + \theta_{12}), \\ v_{E \rightarrow T_2} &= V_2 \cos(\omega t + \theta_2) \end{aligned}$$

The combined signal,  $v_{T_1 \rightarrow T_2} + v_{E \rightarrow T_2}$ , is in a form  $a \cos(\omega t + \theta_a) + b \cos(\omega t + \theta_b)$ . The amplitude of the resultant signal,  $v_{2,k}$ , is then expressed as

$$\begin{aligned} v_{2,k}^2 &= V_1^2 |1 - \Gamma_{1,k}|^2 \alpha_{12}^2 + V_2^2 \\ &+ 2V_1 |1 - \Gamma_{1,k}| \alpha_{12} V_2 \cos(\theta_1 + \theta_{12} + \angle(1 - \Gamma_{1,k}) - \theta_2). \end{aligned}$$

Assuming  $V_2 \gg V_1(1 - \rho_{1,k})\alpha_{12}$ , we can neglect the first RHS term in the above equation and write:

$$\begin{aligned} (v_{2,k})^2 &= V_2^2 \left( 1 + 2 \frac{V_1 |1 - \Gamma_{1,k}| \alpha_{12}}{V_2} \right. \\ &\quad \left. \times \cos(\theta_1 + \theta_{12} + \angle(1 - \Gamma_{1,k}) - \theta_2) \right) \end{aligned}$$

Now we divide both sides of the equation by  $V_2^2$  and take the square root. Further we observe that per the binomial approximation, if  $x \ll 1$ , then  $(1 + 2x)^{1/2} \approx (1 + x)$ . Applying these to the above equation we get

$$\begin{aligned} v_{2,k} &= V_2 + V_1 |1 - \Gamma_{1,k}| \alpha_{12} \cos(\theta_1 + \theta_{12} + \angle(1 - \Gamma_{1,k}) - \theta_2) \\ &= V_2 + V_1 \alpha_{12} \cos(\theta_1 + \theta_{12} - \theta_2) \\ &\quad - V_1 \rho_{1,k} \alpha_{12} \cos(\theta_1 + \theta_{12} - \theta_2 + \phi_{1,k}) \end{aligned}$$

This expression has been used in the determination of the channel parameters  $\alpha_{12}$  and  $\theta_{12}$  in Sections 3 and 4.

## ACKNOWLEDGMENTS

This work is partially supported by NSF grants CNS-1763843 and CNS-1901182.

## REFERENCES

- [1] Abeer Ahmad, Akshay Athalye, Milutin Stanaćević, and Samir R Das. 2019. Collaborative channel estimation in backscattering tag-to-tag networks. In *Proceedings of the 1st ACM International Workshop on Device-Free Human Sensing*. 35–38.
- [2] Abeer Ahmad, Yuanfei Huang, Xiao Sha, Akshay Athalye, Milutin Stanaćević, Samir R Das, and Petar M Djurić. 2020. On measuring Doppler shifts between

- tags in a backscattering tag-to-tag network with applications in tracking. In *ICASSP 2020-2020 IEEE International Conference on Acoustics, Speech and Signal Processing (ICASSP)*. IEEE, 9055–9059.
- [3] Daniel Arnitz, Klaus Witrisal, and Ulrich Muehlmann. 2009. Multifrequency continuous-wave radar approach to ranging in passive UHF RFID. *IEEE transactions on microwave theory and techniques* 57, 5 (2009), 1398–1405.
  - [4] Akshay Athalye, Jinghui Jian, Yasha Karimi, Samir R Das, and Petar M Djurić. 2016. Analog front end design for tags in backscatter-based tag-to-tag communication networks. In *2016 IEEE International Symposium on Circuits and Systems (ISCAS)*. IEEE, 2054–2057.
  - [5] Salah Azzouzi, Markus Cremer, Uwe Dettmar, Rainer Kronberger, and Thomas Knie. 2011. New measurement results for the localization of UHF RFID transponders using an Angle of Arrival (AoA) approach. In *2011 IEEE International Conference on RFID*. 91–97. <https://doi.org/10.1109/RFID.2011.5764607>
  - [6] Dinesh Bharadia, Kiran Raj Joshi, Manikanta Kotaru, and Sachin Katti. 2015. Backfi: High throughput WiFi backscatter. *ACM SIGCOMM Computer Communication Review* 45, 4 (2015), 283–296.
  - [7] Mathieu Bouet and Aldri L. dos Santos. 2008. RFID tags: Positioning principles and localization techniques. In *2008 1st IFIP Wireless Days*. 1–5. <https://doi.org/10.1109/WD.2008.4812905>
  - [8] Kirti Chawla, Christopher McFarland, Gabriel Robins, and Connor Shope. 2013. Real-time RFID localization using RSS. In *2013 International Conference on Localization and GNSS (ICL-GNSS)*. IEEE, 1–6.
  - [9] Gregory Chen, Hassan Ghaed, Razi-ul Haque, Michael Wiecekowsky, Yejoong Kim, Gyouho Kim, David Fick, Daeyeon Kim, Mingoo Seok, Kensall Wise, et al. 2011. A cubic-millimeter energy-autonomous wireless intraocular pressure monitor. In *2011 IEEE International Solid-State Circuits Conference*. IEEE, 310–312.
  - [10] Daniel M Dobkin. 2012. *The RF in RFID: UHF RFID in Practice*. Newnes.
  - [11] Cory Hekimian-Williams, Brandon Grant, Xiuwen Liu, Zhenghao Zhang, and Piyush Kumar. 2010. Accurate localization of RFID tags using phase difference. In *2010 IEEE International Conference on RFID (IEEE RFID 2010)*. IEEE, 89–96.
  - [12] Yuanfei Huang, Akshay Athalye, Samir Das, Petar Djurić, and Milutin Stanačević. 2021. RF Energy Harvesting and Management for Near-zero Power Passive Devices. In *2021 IEEE International Symposium on Circuits and Systems (ISCAS)*. IEEE, 1–5.
  - [13] SkyWorks Inc. [n.d.]. *SMS7630 Datasheet*. [https://www.skyworksinc.com/-/media/SkyWorks/Documents/Products/201-300/Surface\\_Mount\\_Schottky\\_Diodes\\_200041AG.pdf](https://www.skyworksinc.com/-/media/SkyWorks/Documents/Products/201-300/Surface_Mount_Schottky_Diodes_200041AG.pdf)
  - [14] Texas Instruments Inc. [n.d.]. *ADS8860 Datasheet*. <https://www.ti.com/document-viewer/ADS8860/datasheet>
  - [15] Y. Karimi, A. Athalye, S. R. Das, P. M. Djurić, and M. Stanačević. 2017. Design of a backscatter-based Tag-to-Tag system. In *2017 IEEE International Conference on RFID (RFID)*. 6–12. <https://doi.org/10.1109/RFID.2017.7945579>
  - [16] Yasha Karimi, Yuanfei Huang, Akshay Athalye, Samir Das, Petar Djurić, and Milutin Stanačević. 2019. Passive wireless channel estimation in RF tag network. In *2019 IEEE International Symposium on Circuits and Systems (ISCAS)*. IEEE, 1–5.
  - [17] Artur Koch and Andreas Zell. 2016. RFID-enabled location fingerprinting based on similarity models from probabilistic similarity measures. In *2016 IEEE International Conference on Robotics and Automation (ICRA)*. IEEE, 4557–4563.
  - [18] Chenyang Li, Lingfei Mo, and Dongkai Zhang. 2019. Review on UHF RFID localization methods. *IEEE Journal of Radio Frequency Identification* 3, 4 (2019), 205–215.
  - [19] Gang Li, Daniel Arnitz, Randolph Ebel, Ulrich Muehlmann, Klaus Witrisal, and Martin Vossiek. 2011. Bandwidth dependence of CW ranging to UHF RFID tags in severe multipath environments. In *2011 IEEE International Conference on RFID*. IEEE, 19–25.
  - [20] Xin Li, Yimin Zhang, and Moeness G Amin. 2009. Multifrequency-based range estimation of RFID tags. In *2009 IEEE International Conference on RFID*. IEEE, 147–154.
  - [21] Vincent Liu, Aaron Parks, Vamsi Talla, Shyamnath Gollakota, David Wetherall, and Joshua R Smith. 2013. Ambient backscatter: Wireless communication out of thin air. *ACM SIGCOMM Computer Communication Review* 43, 4 (2013), 39–50.
  - [22] Jiaqing Luo, Shijie Zhou, Hongrong Cheng, Yongjian Liao, and Kai Bu. 2015. A Range-Free Localization of Passive RFID Tags Using Mobile Readers. In *2015 IEEE 12th International Conference on Mobile Ad Hoc and Sensor Systems*. 445–446. <https://doi.org/10.1109/MASS.2015.34>
  - [23] Yunfei Ma, Xiaonan Hui, and Edwin C Kan. 2016. 3D real-time indoor localization via broadband nonlinear backscatter in passive devices with centimeter precision. In *Proceedings of the 22nd Annual International Conference on Mobile Computing and Networking*. 216–229.
  - [24] Yunfei Ma, Nicholas Selby, and Fadel Adib. 2017. Minding the billions: Ultra-wideband localization for deployed RFID tags. In *Proceedings of the 23rd annual international conference on mobile computing and networking*. 248–260.
  - [25] Amjad Yousef Majid, Michel Jansen, Guillermo Ortas Delgado, Kasim Sinan Yildirim, and Przemyslaw Pawełczak. 2019. Multi-hop backscatter tag-to-tag networks. In *IEEE INFOCOM 2019-IEEE Conference on Computer Communications*. IEEE, 721–729.
  - [26] Spyros Megalou, Anastasios Tzitzis, Stavroula Siachalou, Traianos Yioultsis, John Sahalos, Emmanouil Tzardoulis, Alexandros Filotheou, Andreas Symeonidis, Loukas Petrou, Aggelos Bletsas, et al. 2019. Fingerprinting Localization of RFID tags with Real-Time Performance-Assessment, using a Moving Robot. In *2019 13th European Conference on Antennas and Propagation (EuCAP)*. IEEE, 1–5.
  - [27] Robert Miesen, Fabian Kirsch, and Martin Vossiek. 2011. Holographic localization of passive UHF RFID transponders. In *2011 IEEE International Conference on RFID*. 32–37. <https://doi.org/10.1109/RFID.2011.5764633>
  - [28] Robert Miesen, Fabian Kirsch, and Martin Vossiek. 2013. UHF RFID localization based on synthetic apertures. *IEEE Transactions on Automation Science and Engineering* 10, 3 (2013), 807–815.
  - [29] Andrea Motroni, Paolo Nepa, Alice Buffi, and Bernardo Tellini. 2019. A Phase-Based Method for Mobile Node Localization through UHF-RFID Passive Tags. In *2019 IEEE International Conference on RFID Technology and Applications (RFID-TA)*. 470–475. <https://doi.org/10.1109/RFID-TA.2019.8892264>
  - [30] Andrea Motroni, Paolo Nepa, Valerio Magnago, Alice Buffi, Bernardo Tellini, Daniele Fontanelli, and David Macii. 2018. SAR-Based Indoor Localization of UHF-RFID Tags via Mobile Robot. In *2018 International Conference on Indoor Positioning and Indoor Navigation (IPIN)*. 1–8. <https://doi.org/10.1109/IPIN.2018.8533847>
  - [31] Pavel V Nikitin, Rene Martinez, Shashi Ramamurthy, Hunter Leland, Gary Spiess, and KVS Rao. 2010. Phase based spatial identification of UHF RFID tags. In *2010 IEEE International Conference on RFID (IEEE RFID 2010)*. IEEE, 102–109.
  - [32] Pavel V Nikitin, Shashi Ramamurthy, Rene Martinez, and KV Seshagiri Rao. 2012. Passive tag-to-tag communication. In *2012 IEEE international conference on RFID (RFID)*. IEEE, 177–184.
  - [33] Andreas Parr, Robert Miesen, and Martin Vossiek. 2013. Inverse SAR approach for localization of moving RFID tags. In *2013 IEEE International Conference on RFID (RFID)*. IEEE, 104–109.
  - [34] Ales Povalac and Jiri Sebesta. 2011. Phase difference of arrival distance estimation for RFID tags in frequency domain. In *2011 IEEE International Conference on RFID-Technologies and Applications*. IEEE, 188–193.
  - [35] Jihoon Ryoo, Jinghui Jian, Akshay Athalye, Samir R Das, and Milutin Stanačević. 2018. Design and Evaluation of “BTNN”: A Backscattering Tag-to-Tag Network. *IEEE Internet of Things Journal* 5, 4 (2018), 2844–2855.
  - [36] Jihoon Ryoo, Yasha Karimi, Akshay Athalye, Milutin Stanačević, Samir R Das, and Petar Djurić. 2018. BARNET: Towards activity recognition using passive backscattering tag-to-tag network. In *Proceedings of the 16th Annual International Conference on Mobile Systems, Applications, and Services*. 414–427.
  - [37] Martin Scherhaeufl, Markus Pichler, Erwin Schimbaeck, Dominik J Mueller, Andreas Ziroff, and Andreas Stelzer. 2013. Indoor localization of passive UHF RFID tags based on phase-of-arrival evaluation. *IEEE Transactions on Microwave Theory and Techniques* 61, 12 (2013), 4724–4729.
  - [38] Martin Scherhaeufl, Markus Pichler, and Andreas Stelzer. 2014. Localization of passive UHF RFID tags based on inverse synthetic apertures. In *2014 IEEE International Conference on RFID (IEEE RFID)*. IEEE, 82–88.
  - [39] Junyang Shen, Andreas F Molisch, and Jussi Salmi. 2012. Accurate passive location estimation using TOA measurements. *IEEE Transactions on Wireless Communications* 11, 6 (2012), 2182–2192.
  - [40] Zhe Shen, Akshay Athalye, and Petar M Djurić. 2016. Phase cancellation in backscatter-based tag-to-tag communication systems. *IEEE Internet of Things Journal* 3, 6 (2016), 959–970.
  - [41] Stavroula Siachalou, Spyros Megalou, Anastasios Tzitzis, Emmanouil Tzardoulis, Aggelos Bletsas, John Sahalos, Traianos Yioultsis, and Antonis G. Dimitriou. 2019. Robotic Inventorying and Localization of RFID Tags, Exploiting Phase-Fingerprinting. In *2019 IEEE International Conference on RFID Technology and Applications (RFID-TA)*. 362–367. <https://doi.org/10.1109/RFID-TA.2019.8892183>
  - [42] Skyworks Inc. [n.d.]. *SKY 13404 0.4-2.7 GHz SP10T Switch with GPIO Interface*. Skyworks Inc. <https://www.skyworksinc.com/-/media/7D48A6DF3B4D40A69D0127FEC430435D.ashx>
  - [43] Milutin Stanačević, Akshay Athalye, Zygmont J Haas, Samir R Das, and Petar M Djurić. 2020. Backscatter Communications with Passive Receivers: From Fundamentals to Applications. *ITU Journal on Future and Evolving Technologies* 1, 1 (2020).
  - [44] STMicroelectronics. [n.d.]. *STM32F205RET6 Datasheet*. <https://www.st.com/resource/en/datasheet/stm32f205re.pdf>
  - [45] Saurav Subedi, Eric Pauls, and Yimin D Zhang. 2017. Accurate localization and tracking of a passive RFID reader based on RSSI measurements. *IEEE Journal of Radio Frequency Identification* 1, 2 (2017), 144–154.
  - [46] Stewart J Thomas and Matthew S Reynolds. 2012. A 96 Mbit/sec, 15.5 pJ/bit 16-QAM modulator for UHF backscatter communication. In *2012 IEEE International Conference on RFID (RFID)*. IEEE, 185–190.
  - [47] Nguyen Van Huynh, Dinh Thai Hoang, Xiao Lu, Dusit Niyato, Ping Wang, and Dong In Kim. 2018. Ambient backscatter communications: A contemporary survey. *IEEE Communications Surveys & Tutorials* 20, 4 (2018), 2889–2922.
  - [48] Jue Wang and Dina Katabi. 2013. Dude, where’s my card? RFID positioning that works with multipath and non-line of sight. In *Proceedings of the ACM SIGCOMM 2013 conference on SIGCOMM*. 51–62.

- [49] Jue Wang, Deepak Vasishth, and Dina Katabi. 2014. RF-IDraw: virtual touch screen in the air using RF signals. In *Proceedings of the 2014 ACM conference on SIGCOMM*. ACM, Chicago Illinois USA, 235–246. <https://doi.org/10.1145/2619239.2626330>
- [50] Haibing Wu, Bo Tao, Zeyu Gong, Zhouping Yin, and Han Ding. 2019. A Fast UHF RFID Localization Method Using Unwrapped Phase-Position Model. *IEEE Transactions on Automation Science and Engineering* 16, 4 (2019), 1698–1707. <https://doi.org/10.1109/TASE.2019.2895104>
- [51] Xiang Wu, Fangming Deng, and Zhongbin Chen. 2018. RFID 3D-LANDMARC localization algorithm based on quantum particle swarm optimization. *Electronics* 7, 2 (2018), 19.
- [52] Huatao Xu, Dong Wang, Run Zhao, and Qian Zhang. 2019. FaHo: deep learning enhanced holographic localization for RFID tags. In *Proceedings of the 17th Conference on Embedded Networked Sensor Systems*. 351–363.
- [53] Huatao Xu, Run Zhao, Qian Zhang, and Dong Wang. 2018. PRMS: Phase and RSSI Based Localization System for Tagged Objects on Multilayer with a Single Antenna. In *Proceedings of the 21st ACM International Conference on Modeling, Analysis and Simulation of Wireless and Mobile Systems* (Montreal, QC, Canada) (*MSWIM '18*). Association for Computing Machinery, New York, NY, USA, 351–355. <https://doi.org/10.1145/3242102.3242138>
- [54] Lei Yang, Yekui Chen, Xiang-Yang Li, Chaowei Xiao, Mo Li, and Yunhao Liu. 2014. Tagoram: real-time tracking of mobile RFID tags to high precision using COTS devices. In *Proceedings of the 20th annual international conference on Mobile computing and networking*. ACM, Maui Hawaii USA, 237–248. <https://doi.org/10.1145/2639108.2639111>
- [55] Fei Yuan. 2011. *CMOS Circuits for Passive Wireless Microsystems*. Springer New York, New York, NY. 49–59 pages. [https://doi.org/10.1007/978-1-4419-7680-2\\_3](https://doi.org/10.1007/978-1-4419-7680-2_3)
- [56] Pengyu Zhang, Dinesh Bharadia, Kiran Joshi, and Sachin Katti. 2016. HitchHike: Practical Backscatter Using Commodity WiFi. In *Proceedings of the 14th ACM Conference on Embedded Network Sensor Systems CD-ROM* (Stanford, CA, USA) (*SenSys '16*). New York, NY, USA, 259–271.
- [57] Pengyu Zhang, Colleen Josephson, Dinesh Bharadia, and Sachin Katti. 2017. Freerider: Backscatter communication using commodity radios. In *Proceedings of the 13th International Conference on emerging Networking EXperiments and Technologies*. 389–401.
- [58] Yunlei Zhang, Yongtao Ma, Xinlong Miao, Shuai Zhang, and Bobo Wang. 2019. Multipath Mitigation Algorithm for Multifrequency-Based Ranging via Convex Relaxation in Passive UHF RFID. *IEEE Internet of Things Journal* 6, 1 (2019), 744–752. <https://doi.org/10.1109/JIOT.2018.2856242>
- [59] Yang Zhao, Kaihua Liu, Yongtao Ma, Zheng Gao, Yangguang Zang, and Jianfu Teng. 2017. Similarity Analysis-Based Indoor Localization Algorithm With Backscatter Information of Passive UHF RFID Tags. *IEEE Sensors Journal* 17, 1 (2017), 185–193. <https://doi.org/10.1109/JSEN.2016.2624314>
- [60] Yiyang Zhao, Yunhao Liu, and Lionel M Ni. 2007. VIRE: Active RFID-based localization using virtual reference elimination. In *2007 International Conference on Parallel Processing (ICPP 2007)*. IEEE, 56–56.
- [61] Chenming Zhou and Joshua D. Griffin. 2012. Accurate Phase-Based Ranging Measurements for Backscatter RFID Tags. *IEEE Antennas and Wireless Propagation Letters* 11 (2012), 152–155. <https://doi.org/10.1109/LAWP.2012.2186110>
- [62] Chenming Zhou and Joshua D Griffin. 2018. Phased-based composite ranging for backscatter RF tags: System analysis and measurements. *IEEE Transactions on Antennas and Propagation* 66, 8 (2018), 4202–4212.